International Journal of
Radiation Oncology
biology • physics

www.redjournal.org

Clinical Investigation: Thoracic Cancer

Quantification of the Variability of Diaphragm Motion and Implications for Treatment Margin Construction

Simon Rit, Ph.D., Marcel van Herk, Ph.D., Lambert Zijp, B.Sc., and Jan-Jakob Sonke, Ph.D.

From the Department of Radiation Oncology, The Netherlands Cancer Institute-Antoni van Leeuwenhoek Hospital, Amsterdam, The Netherlands

Received Apr 20, 2010, and in revised form Jun 7, 2011. Accepted for publication Jun 29, 2011

Summary

This study quantifies the variability of diaphragm motion in the craniocaudal direction during free-breathing radiotherapy of lung cancer patients. Using the diaphragm as a surrogate for targets moving with respiration, asymmetric treatment margins were constructed to account for geometric uncertainties in the cranial and the caudal directions. It was found that the respiratory motion is more irregular during the fractions than between the fractions and that the probability density function of the respiratory motion is asymmetrically distributed. Both aspects have a limited impact on dose distributions and inferred margins, and respiratory motion is adequately

Purpose: To quantify the variability of diaphragm motion during free-breathing radiotherapy of lung patients and its effect on treatment margins to account for geometric uncertainties.

Methods and Materials: Thirty-three lung cancer patients were analyzed. Each patient had 5−19 cone-beam scans acquired during different treatment fractions. The craniocaudal position of the diaphragm dome on the same side as the tumor was tracked over 2 min in the projection images, because it is both easily visible and a suitable surrogate to study the variability of the tumor motion and its impact on treatment margins. Intra-acquisition, inter-acquisition, and inter-patient variability of the respiratory cycles were quantified separately, as were the probability density functions (PDFs) of the diaphragm position over each cycle, each acquisition, and each patient. Asymmetric margins were simulated using each patient PDF and compared to symmetric margins computed from a margin recipe.

Results: The peak-to-peak amplitude variability (1 SD) was 3.3 mm, 2.4 mm, and 6.1 mm for the intra-acquisition, inter-acquisition, and inter-patient variability, respectively. The average PDF of each cycle was similar to the $\sin^4$ function but the PDF of each acquisition was closer to a skew-normal distribution because of the motion variability. Despite large interfraction baseline variability, the PDF of each patient was generally asymmetric with a longer end-inhale tail because the end-exhale position was more stable than the end-inhale position. The asymmetry of the PDF required asymmetric margins around the time-averaged position to account for the position uncertainty but the average difference was 1.0 mm (range, 0.0−4.4 mm) for a sharp penumbra and an idealized online setup correction protocol.

Conclusion: The respiratory motion is more irregular during the fractions than between the fractions. The PDF of the respiratory motion is asymmetrically distributed. Both the intra-acquisition variability and the PDF asymmetry have a limited impact on dose distributions and inferred margins. The use of a margin recipe to account for respiratory motion with an estimate of the average motion amplitude was adequate in almost all patients.

Keywords: Respiratory motion, Cone-beam CT, Geometric uncertainties, Treatment margins, Probability density function

Reprint requests to: Jan-Jakob Sonke, Ph.D., Department of Radiation Oncology, The Netherlands Cancer Institute-Antoni van Leeuwenhoek Hospital, Plesmanlaan 121, 1066CX Amsterdam, The Netherlands. Tel: (+31) 20-5121723; Fax: (+31) 20-6691101; E-mail: j.sonke@nki.nl

Research partly sponsored by grants of Elekta Oncology Systems.

Conflict of interest: none.

Acknowledgments—The authors thank Jamie McClelland for careful reading of the manuscript.

Int J Radiation Oncol Biol Phys, Vol. 82, No. 3, pp. e399−e407, 2012
0360-3016/$ - see front matter
doi:10.1016/j.ijrobp.2011.06.1986

accounted for with symmetric patient-specific margins constructed using a margin recipe and an estimate of the average motion amplitude.

Introduction

Respiratory motion is a source of uncertainty in the radiotherapy of thoracic and upper abdominal cancers and it must be accounted for at every step of the treatment (1). It is mainly driven by the diaphragm but many other organs take part in the process (2). The resulting motion is complex and patient-specific (3, 4).

The respiratory motion is known to be irregular from cycle to cycle. The extent of its variability has been evaluated in a few studies but often on limited datasets (5–9). Repeat four-dimensional (4D) computed tomography (CT) studies are limited to a few cycles per patient for dosimetric reasons (5, 6). Dynamic magnetic resonance imaging (MRI) is a dose-free alternative (7) but datasets are limited to a few patients because it is not part of standard clinical protocols. External signals can be used to obtain larger datasets (8, 9) but they might not be representative of the motion of internal structures (10).

In contrast, 4D cone-beam (CB) CT (11) can provide large datasets for studying the variability of the respiratory motion because CBCTs are routinely acquired for image guidance in our institute. In (4), Sonke *et al.* have measured the trajectories of lung tumors on repeat 4D CBCT acquired at different treatment fractions. However, 4D CBCT reconstructs a single respiratory cycle from projection images acquired over many respiratory cycles, and intra-acquisition variability cannot be captured by 4D CBCT.

The purpose of this study was to quantify the impact of respiratory motion variability during radiotherapy. To that end, the diaphragm was tracked in projection images acquired for 4D CBCT reconstruction. The diaphragm was used because it is both easy to track in the projection images, unlike the tumor, and a good direct surrogate for those tumors that are close to it (12), which are typically the cases with the largest motions (3, 4) and require the largest treatment margins. The obtained probability density function (PDF) was used to evaluate the impact of breathing irregularities and asymmetry on patient-specific treatment margins. The use of real internal motion information provides insights into the effect of the shape of the breathing PDF on margins, but translation to tumor margins is limited to patients where the tumor motion has similar statistical properties (PDF) as the diaphragm motion.

Material and Methods

Patient selection

Patients were selected from the pool of lung cancer patients treated at our radiotherapy department with a conventional fractionation scheme between December 2007 and March 2009. The apex of the closest dome of the diaphragm to the treatment isocenter was manually located on the treatment planning CT (13). We selected 46 patients where the dome was less than 12 cm away from the treatment isocenter to have the dome consistently in the field of view of the scanner.

CB acquisition

CBCT was used for image-guidance using a linac integrated scanner (Elekta Synergy 3.5; Elekta Oncology Systems Ltd., Crawley, West Sussex, UK). Projection images were acquired at 5.5 fps over 200° in 4 min to optimize the sampling for 4D CBCT (11). Each patient had 5–19 CB scans (median = 7) acquired at different treatment fractions during which they breathed freely without coaching. The acquisition parameters were 120 kV, 16 mA, and 20 ms or 40 ms exposure per frame. The resolution of projection images was 512^2 pixels of 0.8^2 mm^2 (0.52^2 mm^2 at the isocenter).

Diaphragm tracking

The diaphragm was tracked from projection to projection using an adapted version of an algorithm developed to extract a respiratory signal from the projection images for 4D CBCT reconstruction (11, 14). The original algorithm proved satisfactory to extract a respiratory phase for 4D CBCT reconstruction during the acquisition; the adaptations were designed for amplitude measurement which requires focusing on one lung.

First, a three-dimensional rectangular region of interest (ROI) was manually drawn on the planning CT around the dome of the diaphragm on the same side as the treatment isocenter. The ROI was projected on the projection images according to the CB geometry, assuming correct patient setup and using the planned position of the isocenter. The rectangle encompassing the projected ROI was used in the next step to crop the diaphragm dome in the projection image (Fig. 1).

Second, each projection was processed as described in Fig. 1 to create one column of the two-dimensional image called the Amsterdam shroud (14). The horizontal axis of this image represents the projection number (*i.e.*, time); the vertical axis represents the position of structures on the craniocaudal axis of the flat panel imager (Fig. 2). In this case, the visible structure is mainly the selected dome except for lateral projections where both domes are superimposed. Therefore, we selected only the anterior projections, acquired with a gantry angle between −140° and −40° (IEC convention), for which the two domes are clearly separated because the kV source is on the anterior side of the patient, the kV beam being orthogonal to the MV beam.

Third, the craniocaudal position of the dome border was automatically processed in every projection by detecting the pixel of each column of the Amsterdam shroud, which has the maximal first derivative value. The extraction was visually validated per CB

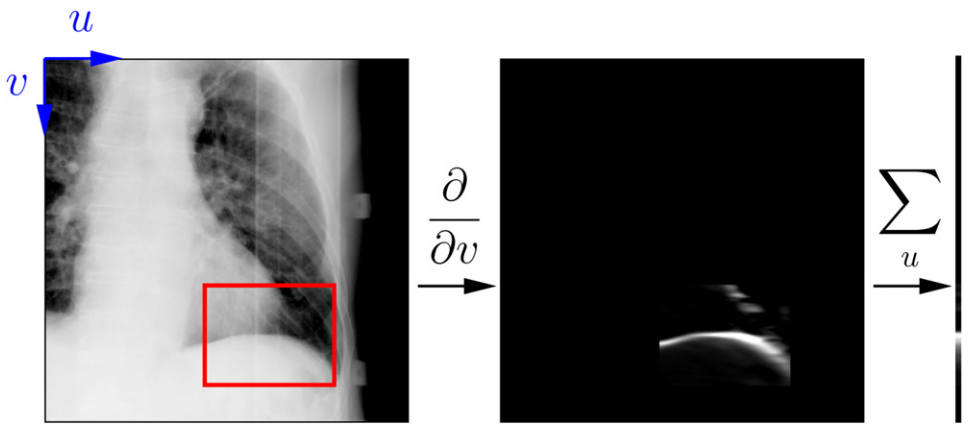

Fig. 1. Example of the processing of a projection image to obtain a column of the Amsterdam shroud (Fig. 2). First, the projection is filtered with a vertical derivative. Only the part in the projected region of interest (ROI) is kept. Second, the sum of the pixel values is taken along each line.

scan by overlaying the processed positions on the Amsterdam shroud (Fig. 2). Patients for which the position extraction failed were excluded from the study (Fig. 3). The pixel coordinate was next converted to a craniocaudal position by taking into account both the geometry of the scanner and the position of the dome identified manually on the planning CT.

The process resulted in a 2-min signal per CB scan describing the craniocaudal position of the selected dome with 0.5-mm resolution at 5.5 Hz (Fig. 2).

Respiratory cycles

A respiratory cycle was defined as the portion of signal between two consecutive end-inhale peaks. End-exhale and end-inhale peaks were located using a robust detection (Fig. 2): peaks were first detected on a smoothed signal to avoid local noise and subsequently adjusted to the position of the signal maximum and the signal minimum between two consecutive end-inhale and end-exhale peaks, respectively. Using the peaks, the cycle length, the peak-to-peak amplitude, and the baseline position were computed for each respiratory cycle. The baseline was defined as the average diaphragm position during the respiratory cycle. The amplitude and baseline statistics (means and standard deviations) were time-weighted using the cycle length to account for cycle length variations.

Probability density function (PDF)

The PDF of the diaphragm position was analyzed at four different scales: the PDF of each cycle (cycle PDF), the PDF of each acquisition (acquisition PDF), and two PDFs for each patient (patient PDF), one simulating an online correction protocol by subtracting from each signal its time average (online protocol) and the other without any data correction (treatment protocol). The

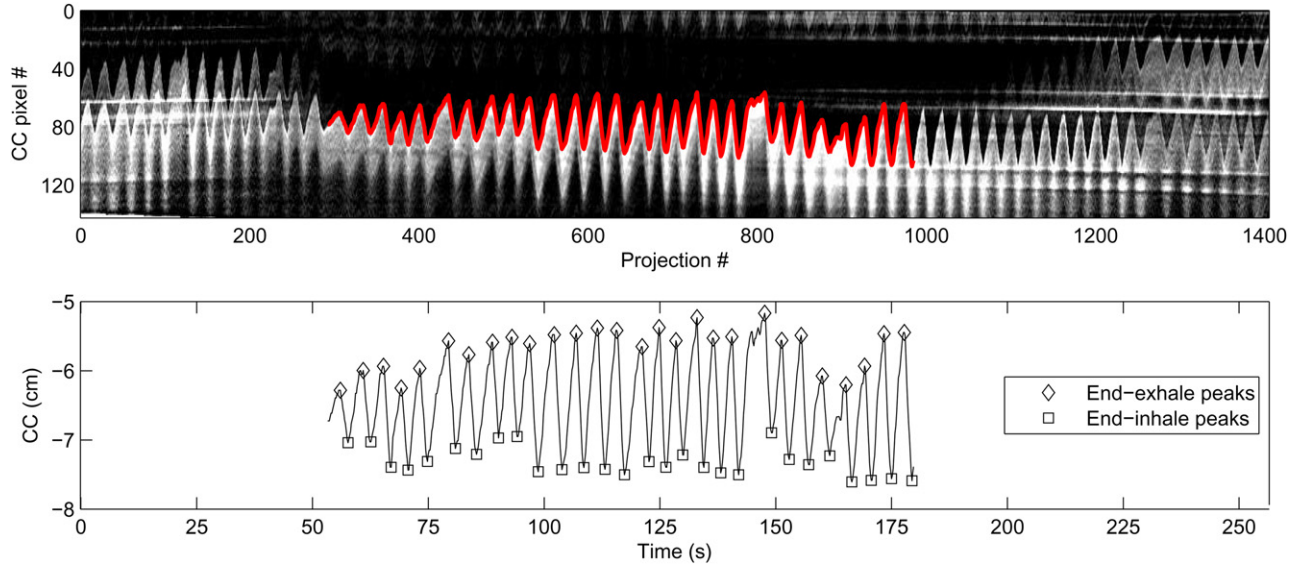

Fig. 2. Top: example of an Amsterdam shroud using the region of interest (ROI) in Fig. 1 for a complete cone beam (CB) scan overlaid with the detected position of the diaphragm dome for gantry angles between −140° and −40°. Bottom: corresponding signal after accounting for the CB geometry and detected peaks. The origin of the coordinate system is the isocenter.

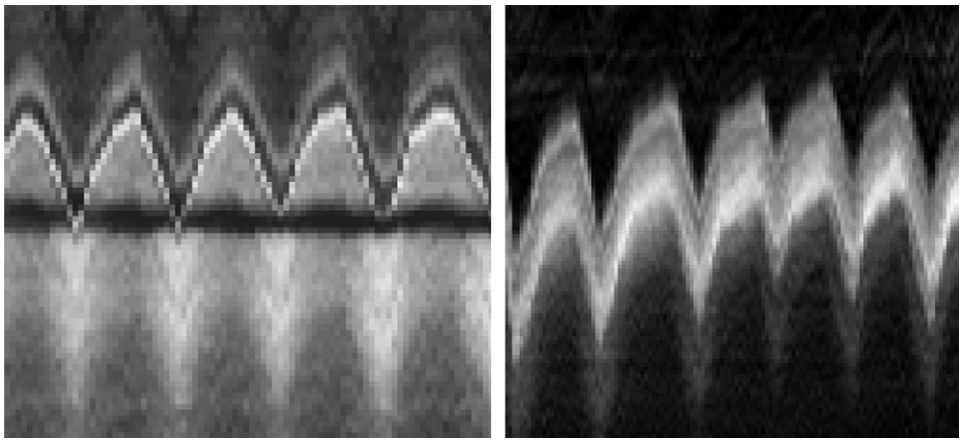

Fig. 3. Amsterdam shrouds of patients eliminated for this study because of difficulties in reliably extracting the craniocaudal position of the diaphragm border. Left: the caudal border of the breast (dark line) is on top of the diaphragm (white line). Right: the apex of the diaphragm dome is not horizontal enough and, consequently, its border is not clearly defined in the Amsterdam shroud.

first two scales only describe the intra-acquisition variability. The last two scales also account for the inter-acquisition variability in two different clinical situations. The online protocol is an idealized simulation of the protocol developed at our institute for stereotactic lung treatments in which the patient setup error is corrected using the time-averaged position of the tumor measured on a 4D CBCT acquired during the same fraction (15). The treatment protocol is the real protocol used for these non-stereotactic patients where the patient setup error is corrected using bony anatomy registrations of three-dimensional CBCTs acquired at previous fractions according to an offline shrinking action-level protocol (4).

The shape of the PDF was illustrated using histograms with 20 bins, computed over all cycles, acquisitions, or patients, depending on the scale. All histograms of a given scale were accumulated bin to bin, which is equivalent to linearly scaling each (cycle, scan, or patient) PDF between the minimum and maximum diaphragm positions. Therefore, the histograms were plotted against the percentage between the minimum (0%) and the maximum (100%) positions, which correspond to the extrema of end-inhale and end-exhale peaks, respectively.

The PDFs were quantitatively characterized with the standard deviation, the skewness, and a normality test. The skewness quantifies the asymmetry of a PDF: a zero skewness value corresponds to a symmetric distribution, positive values correspond to longer end-exhale tails, and, conversely, negative values correspond to longer end-inhale tails. The Shapiro-Wilk test (16) was used to evaluate the normality of the PDF of each cycle and each acquisition signal. We considered the diaphragm motion to be normally distributed if the test statistic was greater than 0.97, similarly to previous work (17).

Treatment margins

Treatment margins are generally derived from measurements of treatment uncertainties assuming normal distributions of the overall uncertainties (18), but the respiratory motion might not be normally distributed (19). Using the measured PDF of the diaphragm dome, we were able to determine the required margins to treat a structure that moves like that dome, without prior assumption regarding its PDF.

An accumulated dose distribution was simulated for each patient using the treatment protocol and the online protocol PDF. The "planned" dose distribution was expressed analytically with a one-dimensional normal cumulative distribution where the σ_p parameter described the dose penumbra, similarly to previous work (18). The dose distribution was convolved with the PDF and the impacts on the cranial and caudal side were analyzed separately. The required margins were computed per patient as the distance between the 95% dose point in the distribution before and after convolution (*i.e.*, with and without uncertainty). The process only provides the margins required to account for the variations during the treatment execution (random) but does not take into account the treatment preparation deviations (systematic) (18).

The resulting margins were compared with the margin obtained from the recipe $1.64(\sqrt{\sigma^2 + \sigma_p^2} - \sigma_p)$ (18), where σ is the standard deviation of the uncertainty, which was obtained from each patient PDF. Note that this margin is tailored to conventional fractionation requiring delivery of at least 95% of the prescribed dose; for stereotactic body radiotherapy prescribing to lower isodose lines, smaller margins are required (15). Similar to the simulation, the systematic component of the variation was not

Table 1 Group mean and variability (1 SD) of the diaphragm motion in the craniocaudal direction measured from the projection images

	Cycle length (s)	Amplitude (mm)	Baseline (mm)	End-exhale (mm)	End-inhale (mm)
Group mean	3.8	16.4	–	–	–
Intra-acquisition variability	0.8	3.1	1.9	1.6	3.2
Inter-acquisition variability	0.6	2.3	4.4	4.3	4.6
Interpatient variability	1.5	5.7	–	–	–

included in the recipe because only the random component was measured in this study (Table 1).

Results

Diaphragm tracking

The selected dome of the diaphragm was successfully tracked in 33 patients resulting in 257 signals. It failed to be tracked in 13 patients for the two reasons illustrated in Fig. 3: the presence of structures in front of the diaphragm, which cannot be separated from the diaphragm dome, or the lack of horizontality of the dome, which results in a fuzzy Amsterdam shroud and prohibits a reliable extraction of the dome position.

The accuracy of the measurement was evaluated on a motion-controlled phantom (Dynamic Thorax Phantom, Model 008A, CIRS, Norfolk, VA) with various motion patterns. The systematic/random errors (*i.e.*, the average/standard deviation of the difference between the measurement and the input motion parameters) were −0.18 sec/0.13 sec for the period and −0.19 mm/0.52 mm for the amplitude.

Motion characteristics

Table 1 provides the average over all patients of the characteristics of the diaphragm motion observed during acquisition. The inter-patient variability was the largest, which confirms that diaphragmatic motion is patient specific. The ranges of the average cycle length and amplitude per patient were 2.0−9.6 sec and 3.8−32.6 mm, respectively.

The intra-acquisition variability of the baseline, end-exhale peaks and end-inhale peaks were significantly different ($p < 10^{-4}$, paired *t*-test). The most stable were the end-exhale peaks and the most unstable were the end-inhale peaks. The baseline variability was in between but closer to the end-exhale variability because of the asymmetric nature of the PDF (see the next section). In contrast, the inter-acquisition variability of the baseline and end-exhale peaks were not significantly different ($p = 0.56$) and the inter-acquisition variability of the end-inhale peaks was mildly significantly different from the inter-acquisition variability of the end-exhale peaks ($p = 0.035$) and baseline ($p = 0.016$), even though the acquisitions were acquired at different fractions.

The combined intra-acquisition and inter-acquisition variability of the amplitude was moderately correlated (Pearson's product-moment correlation coefficient) with the mean amplitude over the cycles (Fig. 4, $r = 0.67$, $p < 10^{-4}$). No statistically significant correlation was observed between the mean amplitude and the variability of the baseline ($r = 0.14$, $p = 0.44$), similarly to previous work (4).

The intra-acquisition variability of the cycle characteristics was significantly different from the inter-acquisition variability ($p < 10^{-4}$). The intra-acquisition variability of the cycle length and peak-to-peak amplitude was larger than the inter-acquisition variability with a group mean difference of 0.2 s and 0.8 mm, respectively. On the contrary, the intra-acquisition variability of the baseline variability was 2.5 mm smaller than the inter-acquisition variability.

The inter-acquisition variability measures the stability of the average characteristics between acquisitions but the stability of the intra-acquisition variability is also important if one wants to design patient specific margins. The variability of the intra-acquisition variability (*i.e.*, the standard deviation per patient of the standard deviation per acquisition of the) length, peak-to-peak amplitude, and baseline between acquisitions of the same patient, was 0.4 sec, 1.6 mm, and 0.8 mm, respectively. It is smaller than other variabilities, which means that the variability of the diaphragm motion is relatively stable between acquisitions of the same patient.

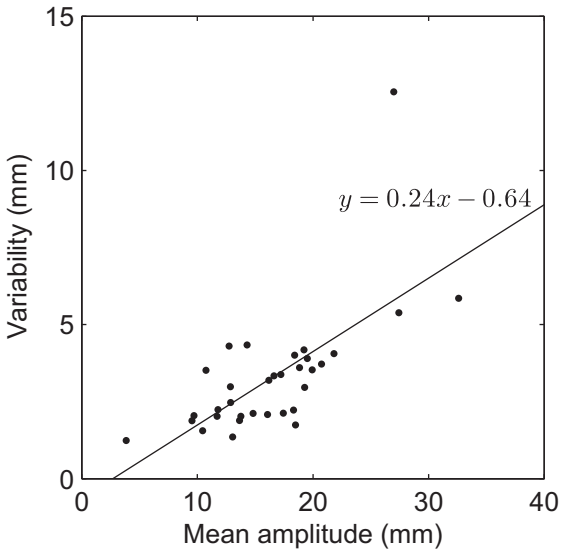

Fig. 4. Plot of the combined intra- and inter-acquisition variability of the peak-to-peak amplitude against the mean peak-to-peak amplitude. Each point corresponds to 1 patient. The line is the best fit in a least-square sense.

PDF

Figure 5 depicts the PDF of the diaphragmatic motion at different scales, and Table 2 contains their quantitative characteristics at each scale.

The average cycle PDF was found to be close to the PDF of the $\sin^4$ function, which is the Lujan model with parameter $n = 2$ (20). It was not normally distributed: the null hypothesis of the Shapiro-Wilk test (the PDF is normally distributed) was accepted for only 3 of the 8,606 respiratory cycles analyzed in this study.

The variability of the respiratory cycles during the acquisition changed the PDF: both end-inhale and end-exhale peaks were blurred (Fig. 5). The end-inhale peak was blurred out while the end-exhale peak was still visible because the intra-acquisition variability of the latter was lower (Table 1). Fifty-six acquisition signals (22%) had a normal distributions.

The inter-acquisition variability resulted in PDFs even closer to normal PDFs. The patient PDF without correction (*i.e.*, the treatment protocol), was normally distributed in 21 patients (64%). An in-between shape was obtained when the inter-acquisition baseline variability (Table 1) was canceled out with an ideal online protocol (simulated): only 11 patients (33%) then had a normal PDF. Quantitatively, the online protocol maintained a stronger asymmetry than the treatment protocol and reduced the average standard deviation of the PDF (Table 2). The skewness of the online protocol was even slightly stronger than the skewness of the acquisition PDF (Table 2), which is indicative of a better alignment of end-exhale peaks than end-inhale peaks between acquisitions.

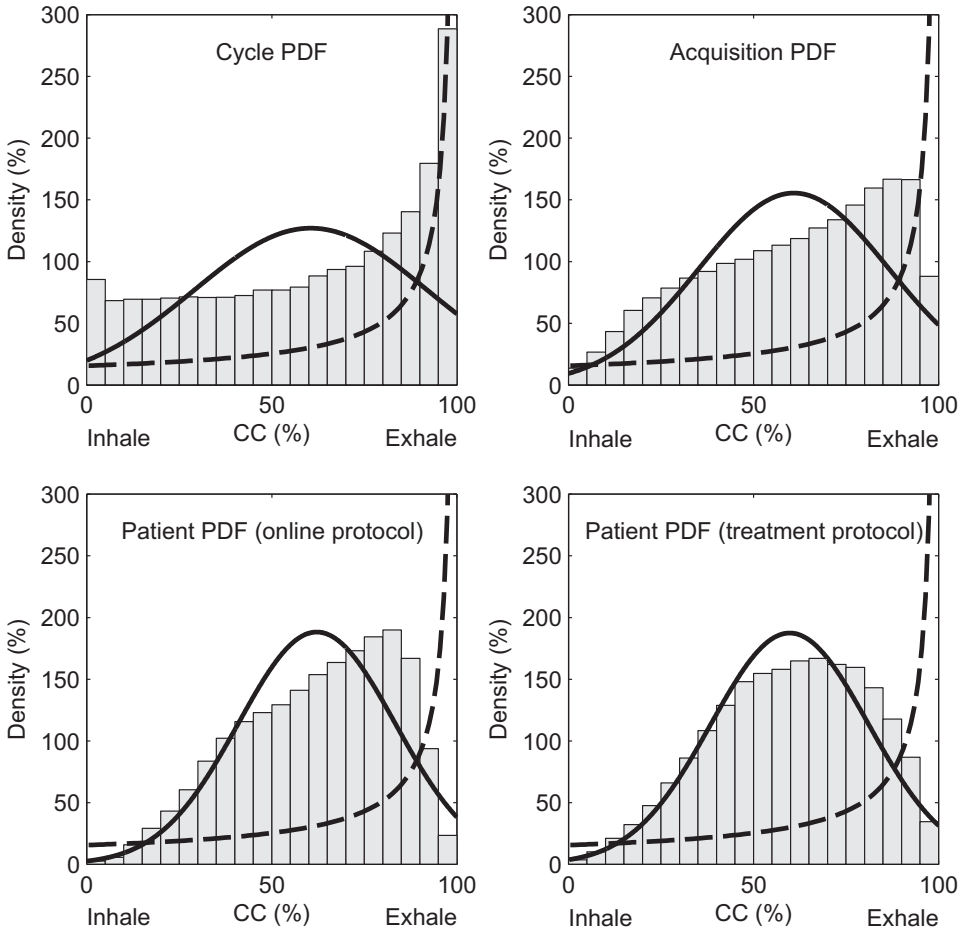

Fig. 5. Histograms (group mean) of the normalized probability density functions (PDF) of the diaphragmatic motion in the craniocaudal (CC) direction at different scales. The solid lines are the PDF of normal distributions with the same mean and variance as the average PDF. The dashed lines are the PDF of the $\sin^4$ function.

Treatment margins

Figure 6 shows the margins that were simulated for the cranial and the caudal field edge, with a lung and a water penumbra, using the patient PDF as well as the symmetric margin given by the recipe of van Herk *et al.* (18). The required margins per patient were systematically larger for the water penumbra ($\sigma_p = 3.2$ mm) than for the lung penumbra ($\sigma_p = 6.4$ mm) because the lung penumbra is broader than the water penumbra (4).

The recipe margin and the cranial and caudal margins were significantly different, even for the offline correction protocol ($p \leq 10^{-3}$, paired t-test). The average differences over the population were smaller or equal to 1.0 mm for both protocols and both penumbras. The maximum difference between the recipe margin and the caudal edge was 4.0 mm and 3.1 mm for the water and the lung penumbras, respectively (Fig. 6, top), in which case the use of the recipe margin would have resulted in treating the caudal edge with 91% and 93% of the dose for the water and the lung penumbras, respectively.

Table 2 Group mean characteristics of the PDF

	1 SD (mm)	Fraction of normal PDF (%)	Skewness (no unit)
Cycle PDF	5.7	0	−0.32
Acquisition PDF	6.1	17	−0.41
Patient PDF—online protocol	6.1	33	−0.43
Patient PDF—offline protocol	7.4	64	−0.27

Abbreviation: PDF = probability density function.

The cranial margin was larger than the caudal margin in at least 27 patients (82%) for all protocols and penumbras, and up to 31 patients (94%) for the online protocol. The recipe margin was between the cranial and the caudal margins in at least 28 patients (85%) and was overestimated in the other patients.

In clinical practice, the PDF is not known but the margin can be computed from the same recipe with an estimate of the standard deviation of the PDF equal to a third of the peak-to-peak amplitude (15). Applying this strategy with the patient mean amplitude gave very similar results as the recipe values based on the measured standard deviation (Fig. 6, solid lines vs. stars). In clinical practice, however, the amplitude is often estimated from a single 4D CT e.g. in previous work (15). Based on a normally distributed peak-to-peak amplitude with a standard deviation proportional to the amplitude using the fit in Fig. 4, 90% of the peak-to-peak amplitude measurements are below A+1.28(0.24A-0.64). Applying the margin recipe to this level, we obtained the

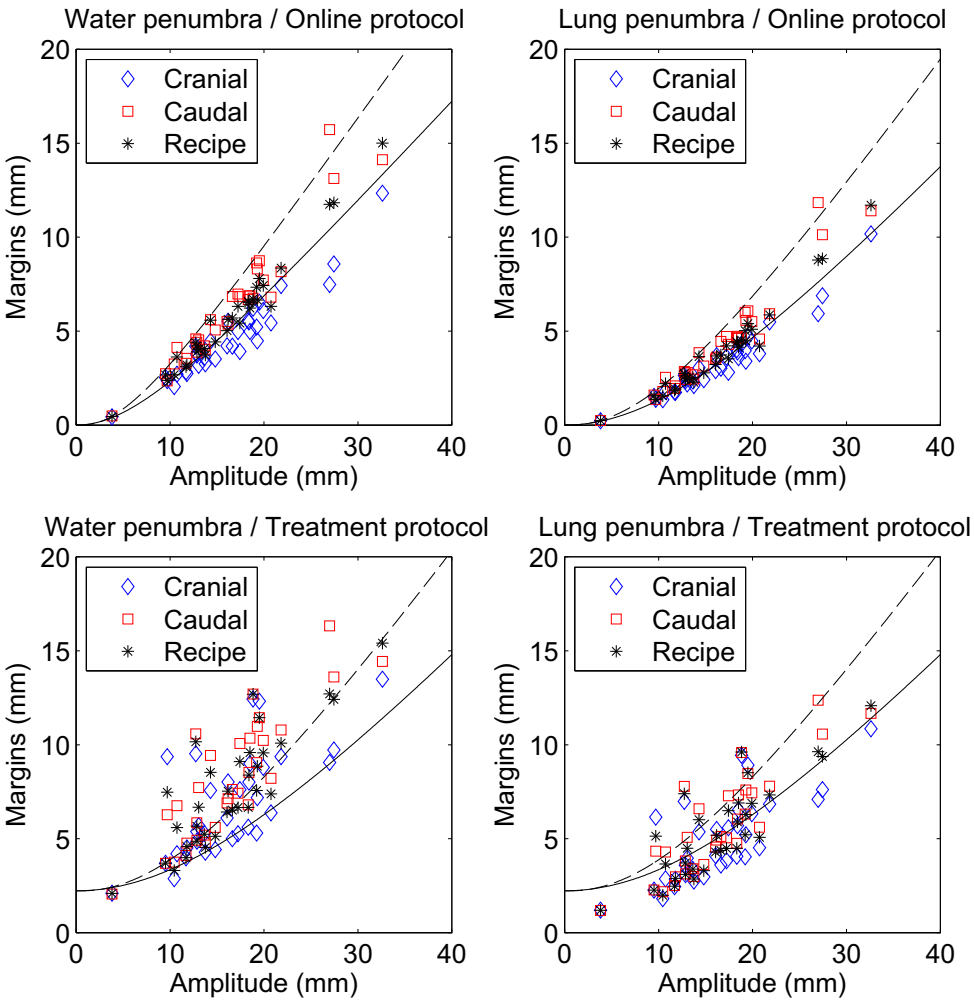

Fig. 6. Plots of the patient-specific margins for random errors (to achieve 95% dose coverage) computed in various ways. The symbols are the margins computed from the Patient probability density function (PDF) with a recipe or simulations (cranial and caudal) against the average peak-to-peak amplitude over the cycles. The solid line plots the margin functions given by the same recipe but using a third of the average amplitude to estimate the standard deviation of the PDF. The dashed line represents the corresponding 90% confidence margin when a single measurement of the amplitude is used. The left and the right column illustrate the margins for the field penumbra corresponding to water-equivalent tissues ($\sigma_p = 3.2$ mm) (18) and lung-equivalent tissues ($\sigma_p = 6.4$ mm) (4), respectively. The top and the bottom rows illustrate the margins for the idealized online protocol and the actual treatment protocol, respectively. The lines in the bottom plots also account for the setup uncertainty via the interfraction baseline variability (Table 1).

margin required to have adequate dose delivery for 90% of the patients (Fig. 6, dashed lines). The difference between the dashed and the solid lines indicates the additional margin required to account for the uncertainty of the peak-to-peak amplitude measured from a single cycle.

Discussion

In this study, we evaluated the impact of breathing irregularities and asymmetry during radiotherapy. To that end, we extracted the motion of one dome of the diaphragm in the craniocaudal direction. Although the results are not directly applicable to other organs moving with the respiration (*e.g.*, lung and upper abdominal tumors), the diaphragm is a good surrogate to describe the variability of tumor motion for most patients (12). Another limitation is that we only tracked the diaphragm motion in the craniocaudal direction. However, it is the main direction of the respiratory motion. Hopefully, current developments will enable markerless measurement in the projection images of the motion of any moving target and organ at risk in every direction (21).

The extraction algorithm failed in 13 patients (28%) because of anatomical specificities (Fig. 3). The specificities were not only pathological but also circumstantial (*e.g.*, the presence of the caudal breast edge in front of the diaphragm in the projection images). However, the failures were also due to lung pathologies in some cases (*e.g.*, atelectases) and the exclusion of such patients might induce a bias in the results because their breathing might be more irregular. Because all patients suffered from lung pathologies, the bias is likely to be limited. Note that the original algorithm only extracts the respiratory phase (11, 14), which has proven to be robust in the vast majority of the patients (4, 15).

Large intra-acquisition variability of the diaphragm motion has been observed (Table 1). This variability implies residual motion

artifacts in 4D imaging methods that assume a regular breathing (*e.g.*, 4D CBCT) (11) and motion-compensated CBCT (22). Moreover, the amplitude variability was larger during each acquisition than between acquisitions, which cannot be observed on 4D CBCT (4) because it reconstructs a single respiratory cycle and only allows measuring the inter-acquisition variability.

The shape of the respiratory cycle is characterized by the position of its peaks and its baseline. The variabilities of those characteristics were noticeably different intra-acquisition but not inter-acquisition (Table 1). Additionally, the inter-acquisition variability of their intra-acquisition variability was relatively low. These observations indicate that the shape of the patient respiratory cycle is less stable during an acquisition than the average shapes over acquisitions taken at different fractions.

Measurement of the cycle-to-cycle motion of a point provides information on the PDF of its spatial position (Fig. 5, Table 2). The PDF of the respiratory cycle has an average shape that approximates a $\sin^4$ model (20) that has been used in many past studies. However, the variability of the respiratory cycles over 2 min changed the shape of the PDF considerably, which was found to be close to a skew-normal distribution (23). As pointed out by George *et al.* (17), inter-fraction variability reduced the asymmetry and produced PDF closer to a normal distribution.

Limited differences were observed between optimal asymmetric margins computed from each patient PDF and symmetric margins computed from a recipe, even for sharp dose distributions and ideal inter-acquisition baseline correction (Fig. 6, top left). Asymmetric margins only provide a benefit for patient specific strategies because the respiratory motion is patient dependent. But it requires pre- or per-treatment measurement of each patient PDF over a multitude of respiratory cycles, which is not easily achievable in clinical practice. Moreover, this study focused on the diaphragm (*i.e.*, one of the points moving the most with respiration) and less asymmetry is expected for less mobile points as random baseline variations would then dominate the PDF (Fig. 6, bottom). Finally, the symmetric margin was between or greater than the asymmetric margins. Although 1 patient is a clear outlier compared with the other ones (Fig. 6, top, second point from the right), the maximal underdosage induced by the use of symmetric margins computed from a recipe was limited to 4% and 2% for the water and the lung penumbra, respectively. For all these reasons, we do not advocate for the use of asymmetric margins in photon beam therapy of targets moving with the respiratory motion but for symmetric margins based on the mean amplitude of the target motion (Fig. 6, solid lines). Systematic inaccuracies have not been studied here and the conclusion might be different if their distribution is also asymmetric.

The mean target amplitude is generally not known before the treatment. To estimate it, we have developed a clinical protocol in our department to measure the tumor amplitude on the planning 4D CT (13). But a 4D CT describes a single respiratory cycle so the measurement has an uncertainty that has to be accounted for (Fig. 6, dashed lines). The effect is clearly not negligible and measuring the mean amplitude from more cycles would be preferable. On the other hand, the uncertainty affects the treatment preparation, which suggests that it should be combined with other systematic errors (18). The inclusion of the uncertainties of patient-specific margins in the margin recipe has not been investigated yet but the impact will be less pronounced if they add up quadratically, as is the case with conventional uncertainties.

Conclusion

Large variability of the diaphragmatic motion has been observed during CB acquisition. The PDF of the diaphragm position during each acquisition is asymmetrically distributed for the majority of the patients. Both the intra-acquisition variability and the PDF asymmetry have a limited impact on dose distributions and inferred margins. The use of a margin recipe with an estimate of the average motion amplitude to account for respiratory motion was adequate in almost all patients.

References

1. Task Group 76. The management of respiratory motion in radiation oncology. Technical report, AAPM; 2005. http://dx.doi.org/10.1118/1.2349696. Date accessed December 23, 2011.
2. Shirato H, Seppenwoolde Y, Kitamura K, Onimura R, Shimizu S. Intrafractional tumor motion: Lung and liver. *Semin Radiat Oncol* 2004;14:10−18.
3. Seppenwoolde Y, Shirato H, Kitamura K, Shimizu S, van Herk M, Lebesque JV, *et al*. Precise and real-time measurement of 3D tumor motion in lung due to breathing and heartbeat, measured during radiotherapy. *Int J Radiat Oncol Biol Phys* 2002;53:822−834.
4. Sonke JJ, Lebesque J, van Herk M. Variability of four-dimensional computed tomography patient models. *Int J Radiat Oncol Biol Phys* 2008;70:590−598.
5. Bosmans G, van Baardwijk A, Dekker A, Ollers M, Boersma L, Minken A, *et al*. Intra-patient variability of tumor volume and tumor motion during conventionally fractionated radiotherapy for locally advanced non-small-cell lung cancer: A prospective clinical study. *Int J Radiat Oncol Biol Phys* 2006;66:748−753.
6. Matsugi K, Narita Y, Sawada A, Nakamura M, Miyabe Y, Matsuo Y, *et al*. Measurement of interfraction variations in position and size of target volumes in stereotactic body radiotherapy for lung cancer. *Int J Radiat Oncol Biol Phys* 2009;75:543−548.
7. Von Siebenthal M, Székely G, Gamper U, Boesiger P, Lomax A, Cattin P. 4D MR imaging of respiratory organ motion and its variability. *Phys Med Biol* 2007;52:1547−1564.
8. Nøttrup TJ, Korreman SS, Pedersen AN, Aarup LR, Nyström H, Olsen M, *et al*. Intra- and interfraction breathing variations during curative radiotherapy for lung cancer. *Radiother Oncol* 2007;84:40−48.
9. Suh Y, Dieterich S, Cho B, Keall PM. An analysis of thoracic and abdominal tumour motion for stereotactic body radiotherapy patients. *Phys Med Biol* 2008;53:3623−3640.
10. Wu H, Zhao Q, Berbeco R, Nishioka S, Shirato H, Jiang S. Gating based on internal/external signals with dynamic correlation updates. *Phys Med Biol* 2008;53:7137−7150.
11. Sonke JJ, Zijp L, Remeijer P, van Herk M. Respiratory correlated cone beam CT. *Med Phys* 2005;32:1176−1186.
12. Cerviño L, Chao A, Sandhu A, Jiang A. The diaphragm as an anatomic surrogate for lung tumor motion. *Phys Med Biol* 2009;54:3529−3541.
13. Wolthaus JWH, Schneider C, Sonke JJ, van Herk M, Belderbos JSA, Rossi MMG, *et al*. Mid-ventilation CT scan construction from four-dimensional respiration-correlated CT scans for radiotherapy planning of lung cancer patients. *Int J Radiat Oncol Biol Phys* 2006;65:1560−1571.
14. Zijp L, Sonke JJ, van Herk M. Extraction of the respiratory signal from sequential thorax cone-beam X-ray images. In: International Conference on the Use of Computers in Radiation Therapy (ICCR). Seoul, Republic of Korea: Jeong Publishing; 2004. p. 507−509.
15. Sonke JJ, Rossi M, Wolthaus J, van Herk M, Damen E, Belderbos J. Frameless stereotactic body radiotherapy for lung cancer using four-dimensional cone beam CT guidance. *Int J Radiat Oncol Biol Phys* 2009;74:567−574.

16. Shapiro SS, Wilk MB. An analysis of variance test for normality (complete samples). *Biometrika* 1965;3:52.
17. George R, Keall PJ, Kini VR, Vedam SS, Ramakrishnan V, Mohan R. Is the diaphragm motion probability density function normally distributed? *Med Phys* 2005;32:396−404.
18. van Herk M, Remeijer P, Rasch C, Lebesque JV. The probability of correct target dosage: Dose-population histograms for deriving treatment margins in radiotherapy. *Int J Radial Oncol Biol Phys* 2000;47:1121−1135.
19. van Herk M, Witte M, van der Geer J, Schneider C, Lebesque JV. Biologic and physical fractionation effects of random geometric errors. *Int J Radiat Oncol Biol Phys* 2003;57:1460−1471.
20. Lujan AE, Larsen EW, Balter JM, Ten Haken RK. A method for incorporating organ motion due to breathing into 3D dose calculations. *Med Phys* 1999;26:715−720. 1999.
21. Zeng R, Fessler JA, Balter JM. Estimating 3-D respiratory motion from orbiting views by tomographic image registration. *IEEE Trans Med Imaging* 2007;26:153−163.
22. Rit S, Wolthaus J, van Herk M, Sonke JJ. On-the-fly motion-compensated cone-beam CT using an a priori model of the respiratory motion. *Med Phys* 2009;36:2283−2296. 2009.
23. Azzalini A. A class of distributions which includes the normal ones. *Scand J Stat* 1985;12:2.